Interpretation of geostationary satellite aerosol optical depth (AOD) over East Asia in relation to fine particulate matter (PM$_{2.5}$): insights from the KORUS-AQ aircraft campaign and seasonality

Shixian Zhai et al.

Correspondence: Shixian Zhai (zhaisx@g.harvard.edu)

Supplementary text: Identification of dust plumes.

Earlier studies (Heim et al., 2020; Peterson et al., 2019) have shown dust events occurring over South Korea during KORUS-AQ. Here we identify dust plumes by examining KORUS-AQ measurements of remote sensed extinction coefficient profiles, in situ aerosol size distributions, and in situ dust and non-dust (sulfate-nitrate-ammonium + organics) aerosol concentrations aboard the DC-8 aircraft. Figure S2 (top panel) shows the evolvement of aerosol extinction coefficient profiles during KORUS-AQ (extinction coefficient profiles on individual days can be found at: https://science-data.larc.nasa.gov/lidar/korus-aq/). High extinction coefficients (> 0.1 km^{-1}) in the lower free troposphere (~ 4 km) were shown on May 5 and 7, reflecting long-range transport of dust in the free troposphere (Heim et al., 2020). On May 12, enhancement of extinction coefficients was detected at 6-8 km.

Figure S3 shows the vertical profiles of cross-section weighted effective radius (R_e), dust, and SNA + organic aerosol concentrations. The cross-section weighted effective radius R_e has been shown as a key parameter relating to the optical properties for aerosols (Chin et al., 2002; Liu et al., 2009), and is calculated as:

$$R_e = \frac{\sum_i N_i D_i^3}{2 * \sum_i N_i D_i^2}$$

Where N_i is the number of particles in the ith size bin, and D_i is the center diameter for the ith size bin. On May 5, R_e starts to increase from 0.2 µm at ~ 4km altitude and reaches to ~ 0.6 µm at ~ 6-7 km altitude. Correspondingly, dust concentration on May 5 increased to ~ 20 µg m^{-3} at ~ 4km (SAGA Ca^{2+} and Na$^+$ measurements at altitude > 4 km on May 5 are missing), with negligible SNA + organic aerosol concentration above 2km (Figure S3c). On May 7, the large R_e (~ 0.6 µm) subsides to the surface, with median dust concentration at the surface reaches near 60 µg m^{-3}, suggesting dust subsidence on this day. May 12 observed large R_e at 6-8 km altitude. Dust concentrations on May 12 start to increase at ~ 5 km, above which SAGA data are mostly missing. Hereafter, we identify data on May 5 and 12 at 6-7 km and on May 7 below 1.5 km in altitude as representative of dust plumes.
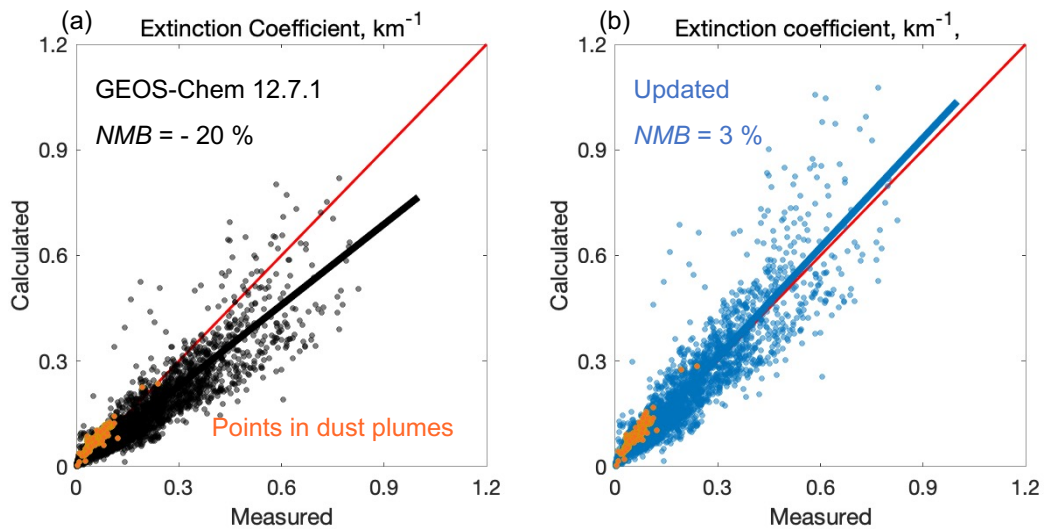
Figure S1. Scatter plots of extinction coefficients between in situ measurements (nephelometer + PSAPs; at ambient RH) and calculations from the measured mass concentrations of major aerosol components (sulfate-nitrate-ammonium, organics, black carbon, and dust), and measured RH, with aerosol optical properties from standard GEOS-Chem version 12.7.1 (panel a) and from updates in this study (panel b; Table 3 in the main text). Normalized mean biases (*NMB*s) inset are for the comparison of calculated and in-situ measured extinction coefficients. No significant bias was seen for measurement in dust plumes.
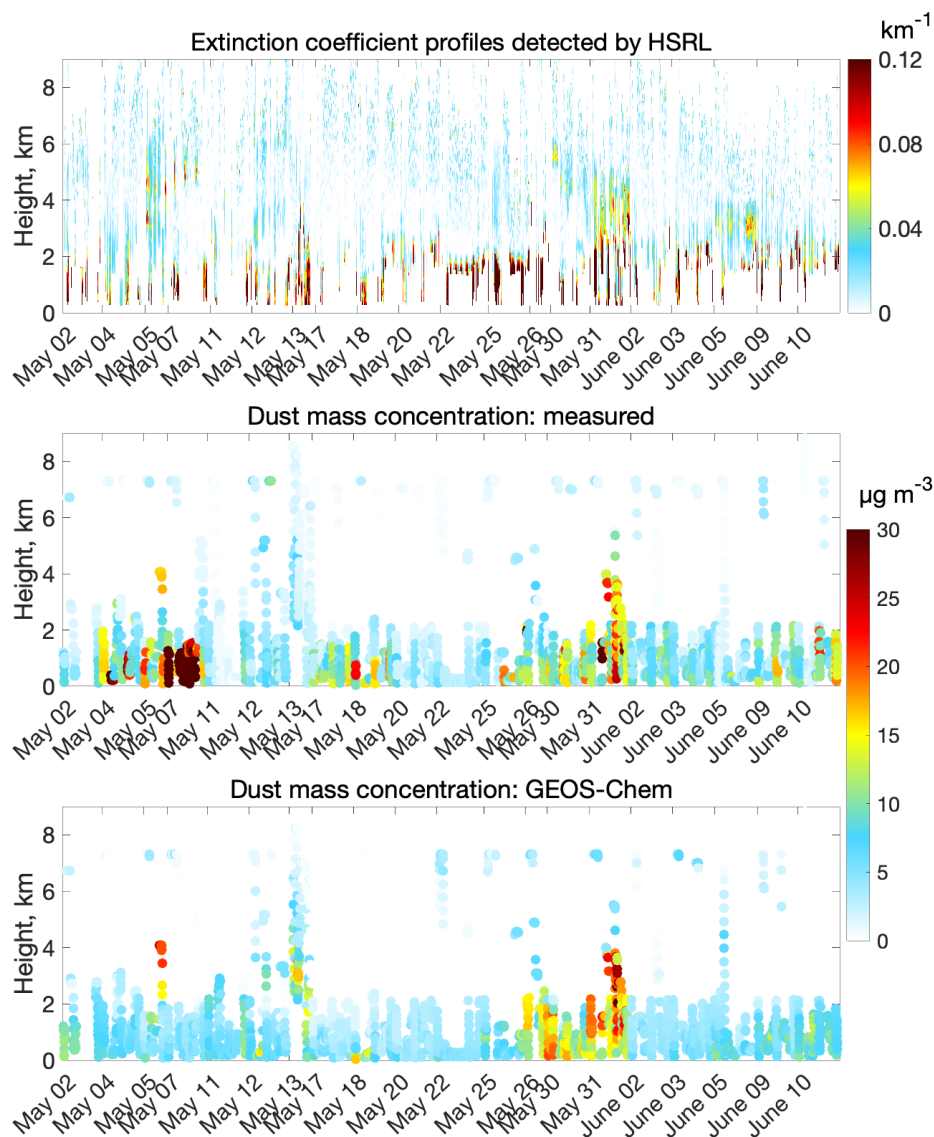
38

39   Figure S2. Extinction coefficient profiles (532 nm) and dust concentration along the flight tracks during KORUS-

40   AQ. The extinction coefficients were detected by High Spectral Resolution Lidar (HSRL). Extinction coefficient

41   profiles on individual days can be found at: https://science-data.larc.nasa.gov/lidar/korus-aq/. Measured dust

42   concentration is derived from SAGA Ca^{2+} and Na^+ as explained in the main text. GEOS-Chem dust is sampled at the

43   flight tracks.

44
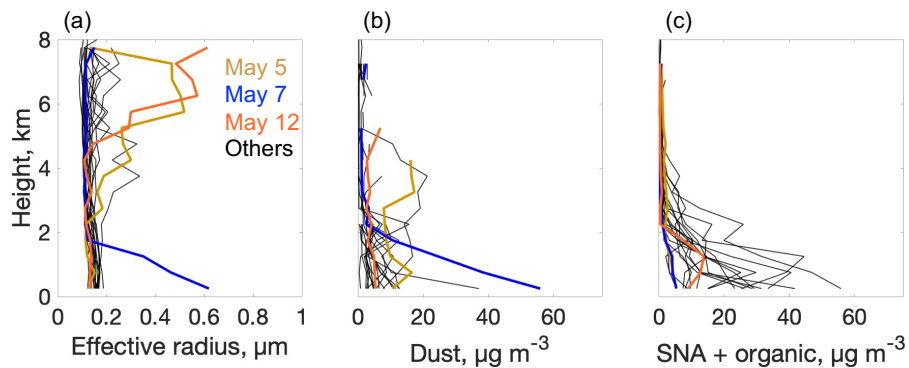
Figure S3. Vertical profiles of measured median (a) cross-section weighted effective radius (R_e), (b) dust concentration, and (c) sulfate-nitrate-ammonium (SNA) + organic aerosol concentration during KORUS-AQ. Profiles on dust events are bold colored. Dust concentration is derived from Ca^{2+} and Na^+ measurements as described in the main text. SNA + organic aerosols are measured by AMS. The incomplete lines for dust concentration profiles are due to missing data. Sampling SNA + organic concentration data at available dust observation points doesn't change the profile features in (c).
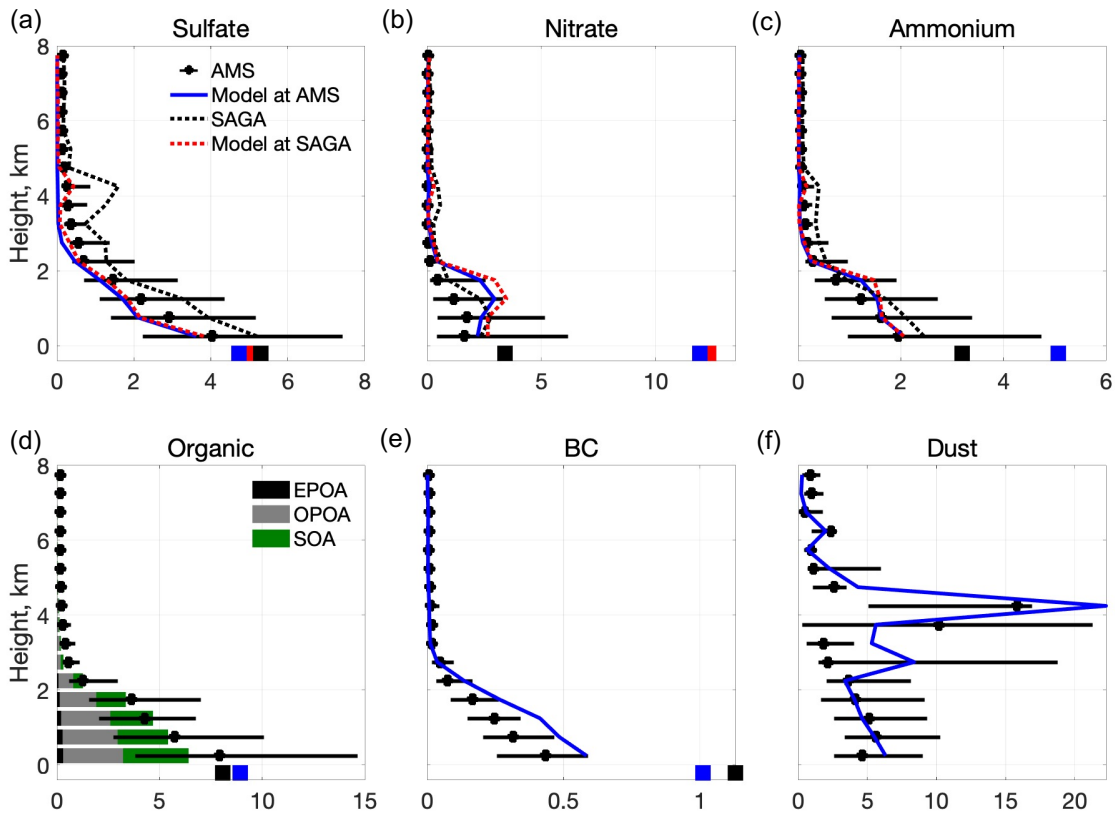
Figure S4. Median vertical profiles of aerosols during KORUS-AQ from measurements (error bars are 25 - 75th percentiles) and GEOS-Chem. For sulfate, nitrate, and ammonium, both AMS and SAGA measurements are shown. Concentration at the surface from both measurements and the model are shown by color filled squares. Modeled sulfate and nitrate at AMS are ammonium associated sulfate and nitrate. Modeled sulfate and nitrate at SAGA include sulfate and nitrate associated with ammonium and dust with geometric diameter < 2.5 μm, to be consistent with SAGA measurements (Table 2 in the main text). Organic aerosol is broken down into freshly emitted primary organic aerosol (EPOA), oxygenated primary organic aerosol (OPOA), and lumped secondary organic aerosol (SOA) by the simple SOA scheme in GEOS-Chem. In the GEOS-Chem simple SOA scheme, 50% primarily emitted organics is assumed to be OPOA (near-field oxidation of EPOA), and the rest 50% organics emitted as EPOA is converted to OPOA with a lifetime of 1.15d. SOA is scaled from biogenic (isoprene, monoterpene, and sesquiterpenes), fire (CO), and anthropogenic (CO) emissions as described by Pai et al. (2020). Vertical profiles are shown for all 20 flights during KORUS-AQ. Surface data are from May 9 to June 10 on flight days, so that median values across sites are slightly different from that inset in Figure 4 in the main text. All data are averaged over 500-m vertical bins. Here and elsewhere, we excluded 3.4% of the data as pollution plumes diagnosed by either NO_2 or SO_2 > 10 ppbv.
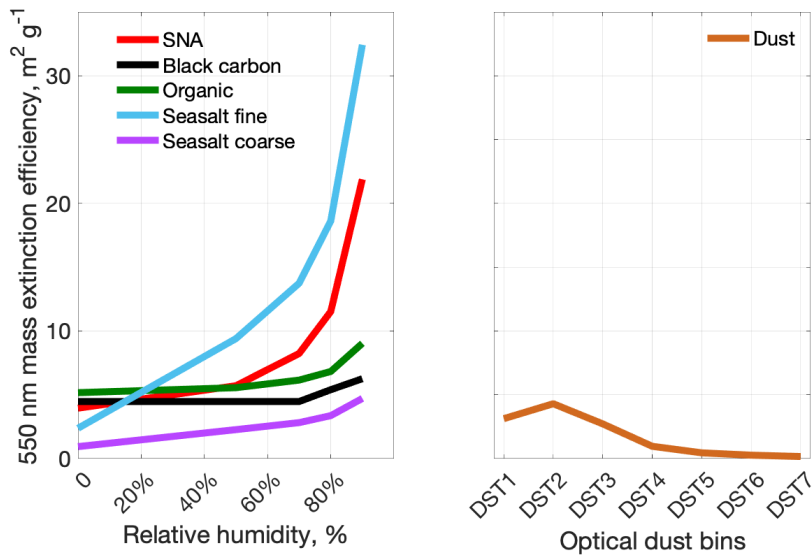
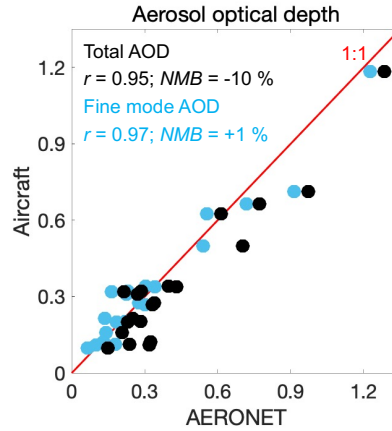Figure S5. Mass extinction efficiency of different areosol components based on GEOS-Chem aerosol optical properties in Table 3 in the main text. The 7 dust size bins (DST1-7) are centered at radii of 0.15, 0.25, 0.4, 0.8, 1.5, 2.5, and 4.0 μm.

Figure S6. Mean aerosol optical depth (AOD) inferred from KORUS-AQ aircraft data for each of the 20 flights over 2 May - 10 June 2016 compared to the mean AOD observed on the flight days at 21 AERONET sites operated across South Korea. AOD from the aircraft data are the integrals of the vertically binned in situ extinction coefficients along the flight tracks. AERONET AOD are daily mean values reported for total aerosol and fine-mode aerosol. The distribution of AERONET sites is shown in Figure 4. Statistics inset are for the correlation coefficient (r) and normalized mean biases (NMBs). Comparison to the AERONET total AOD indicates a normalized mean bias (NMB) of -10%, which might reflect spatial/temporal sampling differences like limited aircraft sampling at surface layer below 150 m and that aircraft AOD do not include aerosol extinctions in the stratosphere (Murphy et al., 2020), but may also be due to a cutoff aerodynamic diameter of ~ 4 μm for the aircraft nephelometers (Mcnaughton et al., 2007). Indeed, the bias disappears when the aircraft AOD is compared to the reported fine-mode AERONET AOD.
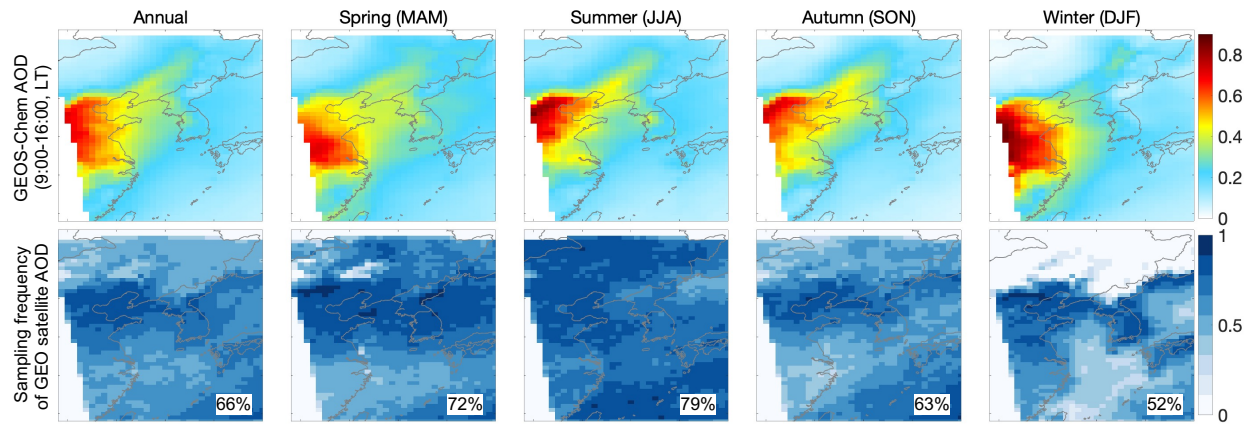
Figure S7. Spatial distributions of 2016 annual and seasonal mean GEOS-Chem all-sky AOD (9:00 - 16:00, LT mean AOD without filtering out cloudy conditions detected by GEO satellites) and the sampling efficiency (proportion of days with successful sampling) of the fused geostationary satellite AOD product.
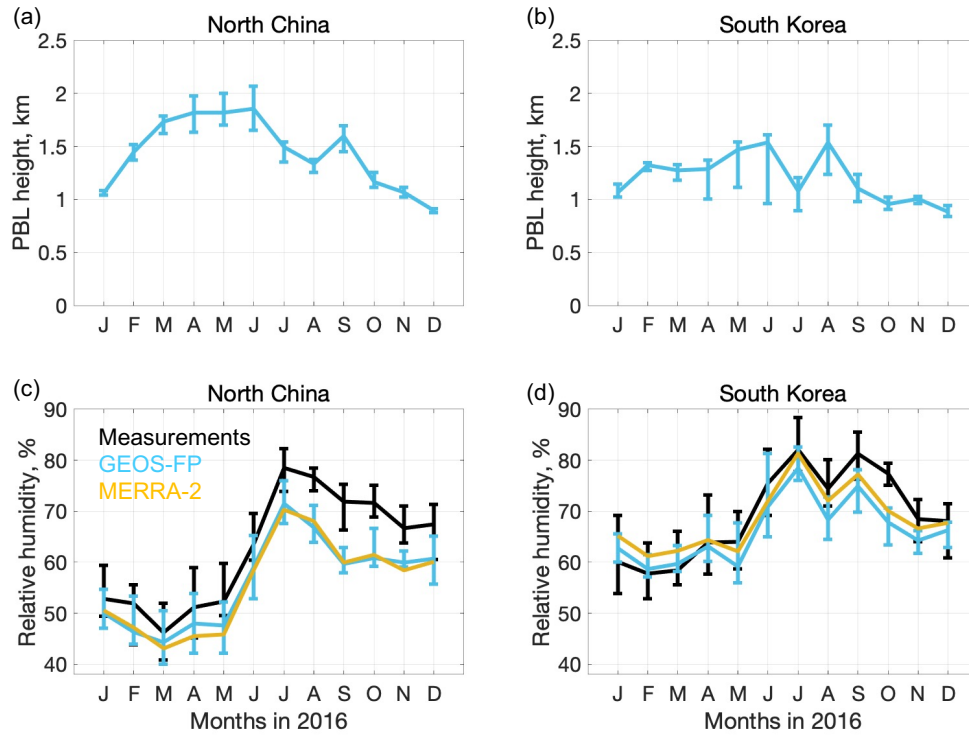
Figure S8. Monthly series of median (error bars: 25th and 75th percentiles) GEOS-FP daytime (9:00-16:00 LT) maximum PBLH heights and daily relative hum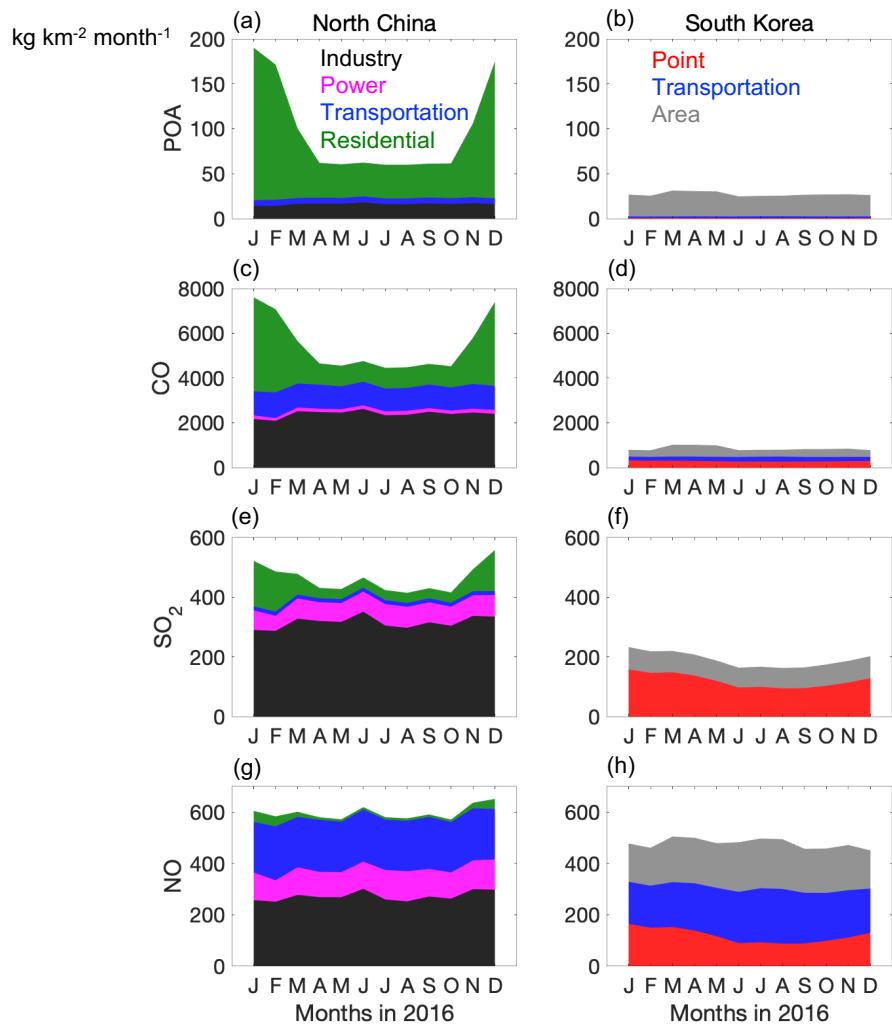idity (RH) over the North China and South Korea regions. The measured RH are from the national climatic datasets of China (data.cma.cn) and South Korea (data.kma.go.kr). RH from MERRA2 is similar to that from GEOS-FP.

Figure S9. Monthly series of sector-specific emission intensities for primary organic aerosol (POA), CO, SO$_2$ and NO over North China and South Korea regions used in driving the GEOS-Chem model. Emissions over North China are from the MEIC emission inventory for 2016 and emissions over South Korea are from the KORUSv5 emission inventory at base year 2015. The two emission inventories are distinguished from different sector categories in this graph. The 'area' source category in KORUSv5 includes residential and scattered low-height industrial combustion and process (Woo et al., 2020). The 'point' source category in KORUSv5 includes large point sources from power plants and industry (Woo et al., 2020).

107   **References**

108   Chin, M., Ginoux, P., Kinne, S., Torres, O., Holben, B. N., Duncan, B. N., Martin, R. V., Logan, J. A., Higurashi,
109   A., and Nakajima, T.: Tropospheric Aerosol Optical Thickness from the GOCART Model and Comparisons with
110   Satellite and Sun Photometer Measurements, J. Atmos. Sci., 59, 461-483, https://doi.org/10.1175/1520-
111   0469(2002)059<0461:TAOTFT>2.0.CO;2, 2002.

112   Heim, E. W., Dibb, J., Scheuer, E., Jost, P. C., Nault, B. A., Jimenez, J. L., Peterson, D., Knote, C., Fenn, M., Hair,
113   J., Beyersdorf, A. J., Corr, C., and Anderson, B. E.: Asian dust observed during KORUS-AQ facilitates the uptake
114   and incorporation of soluble pollutants during transport to South Korea, Atmospheric Environment, 224, 117305,
115   https://doi.org/10.1016/j.atmosenv.2020.117305, 2020.

116   Liu, P., Zhao, C., Liu, P., Deng, Z., Huang, M., Ma, X., and Tie, X.: Aircraft study of aerosol vertical distributions
117   over Beijing and their optical properties, Tellus B: Chemical and Physical Meteorology, 61, 756-767,
118   10.1111/j.1600-0889.2009.00440.x, 2009.

119   McNaughton, C. S., Clarke, A. D., Howell, S. G., Pinkerton, M., Anderson, B., Thornhill, L., Hudgins, C.,
120   Winstead, E., Dibb, J. E., Scheuer, E., and Maring, H.: Results from the DC-8 Inlet Characterization Experiment
121   (DICE): Airborne Versus Surface Sampling of Mineral Dust and Sea Salt Aerosols, Aerosol Sci. Tech., 41, 136-159,
122   https://doi.org/10.1080/02786820601118406, 2007.

123   Murphy, D. M., Froyd, K. D., Bourgeois, I., Brock, C. A., Kupc, A., Peischl, J., Schill, G. P., Thompson, C. R.,
124   Williamson, C. J., and Yu, P.: Radiative and chemical implications of the size and composition of aerosol particles
125   in the existing or modified global stratosphere, Atmos. Chem. Phys. Discuss., 2020, 1-32, 10.5194/acp-2020-909,
126   2020.

127   Pai, S. J., Heald, C. L., Pierce, J. R., Farina, S. C., Marais, E. A., Jimenez, J. L., Campuzano-Jost, P., Nault, B. A.,
128   Middlebrook, A. M., Coe, H., Shilling, J. E., Bahreini, R., Dingle, J. H., and Vu, K.: An evaluation of global organic
129   aerosol schemes using airborne observations, Atmos. Chem. Phys., 20, 2637-2665, https://doi.org/10.5194/acp-20-
130   2637-2020, 2020.

131   Peterson, D. A., Hyer, E. J., Han, S.-O., Crawford, J. H., Park, R. J., Holz, R., Kuehn, R. E., Eloranta, E., Knote, C.,
132   Jordan, C. E., and Lefer, B. L.: Meteorology influencing springtime air quality, pollution transport, and visibility in
133   Korea, Elementa-Sci. Anthrop., 7, 57, https://doi.org/10.1525/elementa.395, 2019.

134   Woo, J.-H., Kim, Y., Kim, H.-K., Choi, K.-C., Eum, J.-H., Lee, J.-B., Lim, J.-H., Kim, J., and Seong, M.:
135   Development of the CREATE Inventory in Support of Integrated Climate and Air Quality Modeling for Asia,
136   Sustainability, 12, 7930, https://doi.org/10.3390/su12197930, 2020.

137